METHODOLOGY

Aerodynamic performance and cooling effect of exhaust passage in steam turbine with new water spray scheme

Lihua Cao[1] · Wanyu Li[1] · Han Du[1]

Abstract

During the actual operation of the power plant, the steam turbine will appear to operate under low load conditions. This paper proposes a novel water spray arrangement for the exhaust channel. Spraying ports are evenly arranged on the cone wall so that the direction of water spraying is opposite to that of the exhaust steam flow (reverse spraying). The feasibility of the nozzle was verified by simulation calculations of existing wind tunnel experiments. The results show that evaporation increases with decreasing load. And the evaporation volume is greater in the reverse spraying than in the down spraying (the direction of water spraying is the same as the direction of steam flow), with a maximum difference of 0.42 kg/s. The deterioration of the aerodynamic performance in the exhaust passage after water spraying can be attributed to the combined effect of the evaporation of water droplets and droplet interference with the flow field. The maximum reduction of 8.17% in the static pressure recovery coefficient in the reverse spray mode increased the total pressure drop by 377.4 Pa. After the water spraying, the temperature dropped significantly compared to before the water spraying. In reverse spraying, the vortex scale in the exhaust passage becomes larger, the return vortex flow increases, the volume absorption ability is stronger, the water droplets and steam contact time is long, good temperature reduction is achieved, and the temperature of the leaf root high-temperature zone is reduced. The maximum difference in temperature drop between the two spraying methods is 56.87 K. The results of this paper provide a reference for the cooling of the exhaust passage when the turbine is operated under low flow conditions for a long time.

1 Introduction

The exhaust passage of the steam turbine consists of a guide ring and a guide cone, which decelerates and expands the steam at the final stage of the turbine and recovers the residual velocity kinetic energy. The commercial CFD code ANSYS CFX18.0 is used to analyze the aaerodynamic performance and temperature reduction effect of the exhaust passage after water spraying, and the Euler–Lagrange method is implemented to calculate the heat and mass transfer in the spray water process.

The exhaust passage is an important part connecting the final stage of the low-pressure cylinder of the turbine and the condenser. Figure 1a shows the structure of the low-pressure exhaust passage. The exhaust passage can decelerate and expand the steam at the end of the turbine and recover the

residual kinetic energy [1]. When the turbine is operated under low load for a long time, it will cause the final stage to enter the blast condition. The power consumption under this condition will increase the exhaust steam temperature. The end of the low-pressure cylinder will be overheated, leading to over-temperature deformation and seriously affecting the turbine's safe operation.

Scholars have recently researched the steam exhaust passages of turbine-blowing conditions. Hu et al. [2] have shown that the diffuser's pressure expansion capacity increases with the inclination angle of the diffuser ring, which improves the flow characteristics in the exhaust passage to a certain extent. Wang et al. [3] analyzed the exhaust cylinder's flow and vortex system characteristics based on the three volumetric flow conditions of 100%, 43.86%, and 21.04%. Moreover, the static pressure recovery coefficient and total pressure loss coefficient distribution laws were obtained. Wang et al. [4] pointed out that as the volumetric flow rate decreases, the streamline distribution in the exhaust passage deteriorates, the streamline turbulence increases, complex vortex systems appear, the flow stability of the outlet

✉ Wanyu Li
  1202300012@neepu.edu.cn

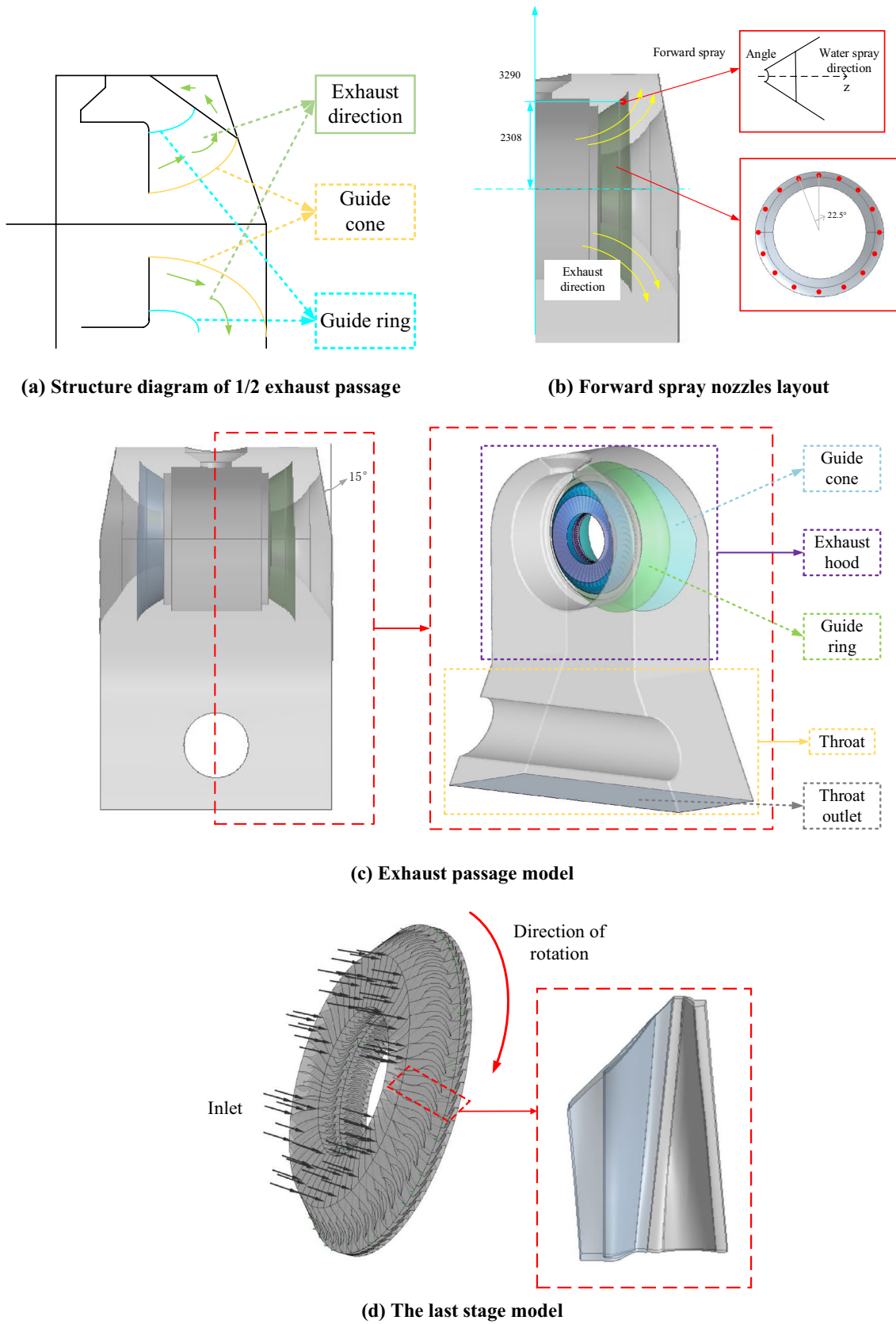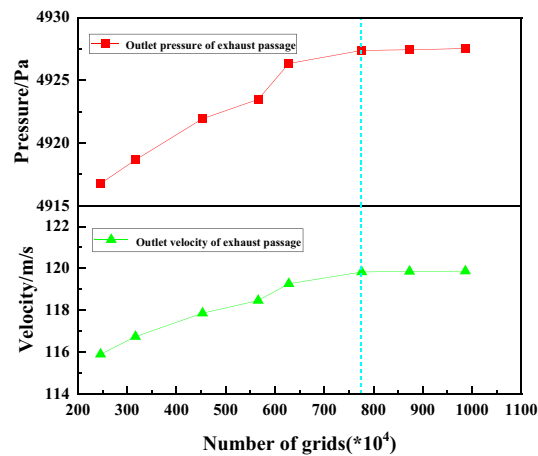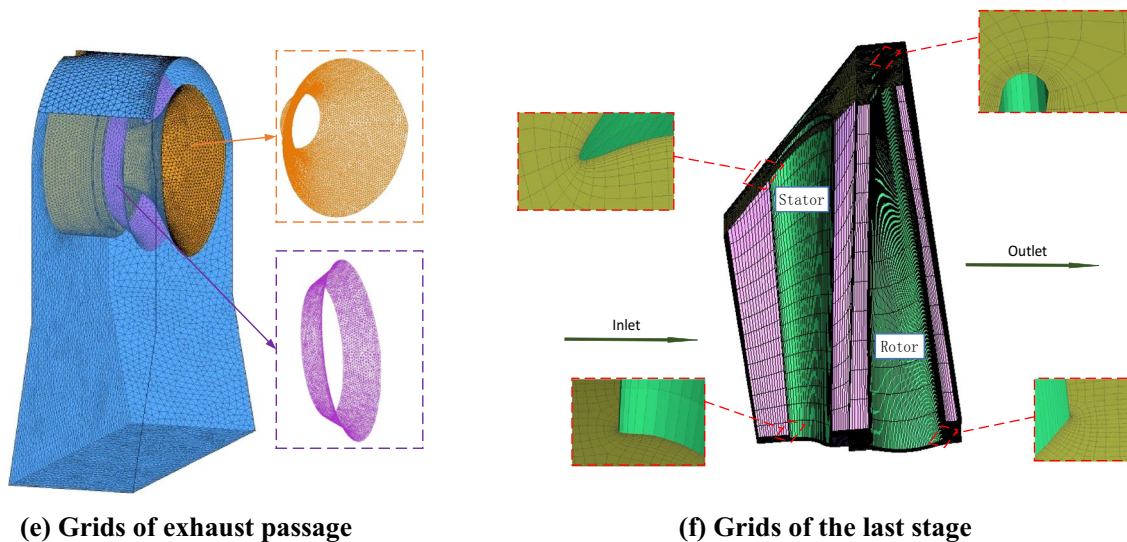1 School of Energy and Power Engineering, Northeast Electric Power University, Jilin 132012, PR China

(a) Structure diagram of 1/2 exhaust passage

(b) Forward spray nozzles layout

(c) Exhaust passage model

(d) The last stage model

Fig. 1 Physical model

(e) Grids of exhaust passage

(f) Grids of the last stage

(g) Verification of grid independence

Fig. 1 (continued)

section decreases, the static pressure recovery coefficient decreases, and the total pressure loss coefficient increases. Cao et al. [5] coupled the turbine's final stage blades to the exhaust passage and studied the final stage flow field on the aerodynamic performance of the discharge channel at small volume flow rates. Beevers et al. [6] proposed that after the final stage reaches the blast condition under small volume flow conditions, the vortex flow between the rotor and fixed blades increases the blade temperature, affecting the blade operation's safety and limiting the turbine's operating range. Li et al. [7] analyzed the changes in thermal parameters and exhaust parameters of the low-pressure cylinder between stages at small-volume flow conditions and the operational risks. They proposed to ensure the low-pressure cylinder's operation safety by increasing temperature measurement points and water spraying for temperature reduction in the exhaust passage.

Therefore, once the turbine is installed, the exhaust passage is equipped with a manufacturer's configuration of water spraying and temperature reduction device, such as the water spraying port on the guide ring shown in Fig. 1b, to ensure the safe operation of the turbine exhaust cylinder under blast conditions. The direction of the water spray is the same as the flow direction of the exhaust steam, i.e., forward spray. However, a more effective and long-running water spraying method should be used when the turbine is operated under blast conditions for a long time.

Water spray to reduce temperature is the spraying of low-temperature water into the flow field that needs to be cooled, and the low-temperature water evaporates to absorb heat. It is a complex heat and mass transfer process due to heat, mass, and momentum exchange between the vapor and liquid droplets. Sureshkumar et al. [8] improved the pressure and flow rate of the water spray under different environments

through wind tunnel experiments to achieve the best cooling effect. The simulation model of bidirectional heat and mass transfer coupling between droplets and air was also established. The simulation results and experimental data were consistent within ± 15% for parallel configuration and ± 30% for counterflow configuration, and the effect of water spraying on the evaporative cooling phenomenon was better investigated by combining experiment and simulation [9] (censored) Sun et al. (censored literature) Sun et al. [10] studied the film layer's formation, fragmentation, and atomization during the spraying process of a full-cone pressure cyclone atomizer, compared the experimental results of spray cooling with the numerical simulation results, and obtained a better agreement. Montazeri et al. [11] calculated the performance of the water spray cooling system by numerical simulation, and the wind tunnel experiments verified that the numerical simulation results were in good agreement with the experimental results, proving that the numerical simulation could predict the water spray cooling process more accurately. Xu et al. [12] used the Euler–Lagrange particle tracking method to study water's heat and mass transfer in the exhaust passage. They predicted the effect of water spray volume on the flow field of the final stage under different conditions. Based on this, the strength performance of the rotor lobe of the final stage under the water spraying and temperature reduction conditions was calculated using the fluid–solid coupling method [13]. Cao et al. [14] analyzed different water spraying methods for small volume flow rates and used the orthogonal test method to derive the optimal water spraying parameters. It is accurate and feasible to carry out the study of water spraying for cooling reduction in the turbine exhaust passage and the final stage under the low flow rate background based on numerical simulation technology.

However, the above studies all focus on the forward spraying method, i.e., the direction of water spraying is the same as the direction of exhaust steam flow, which is used when the turbine exhaust steam temperature is occasionally very high. Water spraying is used when the turbine operates in blast conditions for a long time, the exhaust passage is continuously over-tempered, and the cooling effect of using this water spraying method cannot guarantee the long-term safe operation of the turbine.

Therefore, this paper proposes a new arrangement of exhaust passage water spraying for temperature reduction, in which the water spraying ports are evenly arranged on the cone wall. The nozzle parameters are shown in Table 1. Consequently, the direction of water spraying is opposite to the direction of exhaust steam flow, i.e., reverse spraying. This paper couples the turbine's final stage with the exhaust passage to explore the effect of the new water spraying method on the aerorotor characteristics and cooling effect of the turbine exhaust passage. Moreover, ANSYS CFX software

Table 1 Nozzle parameters

Parameters	Values
Nozzle droplet size	$40\mu m$
Nozzle droplet mass flow rate	0.1628 kg/s
Droplet velocity	60m/s
Spray angle	75°

is used to simulate the flow and heat transfer process in the turbine exhaust passage using the Eulerian-Lagrange particle tracking droplet spraying cooling method. Then, the exhaust passage's aerorotor characteristics and cooling effect are used to provide a long-term solution for the turbine, laying the foundation for the long-term cooling of the exhaust passage under blast operation.

2 Numerical simulation

In this study, the commercial CFD code ANSYS CFX18.0 [15] is used, and the Euler–Lagrange method is implemented to calculate the heat and mass transfer in the spray water process. The effect of droplets on the continuous phase is taken as the source term of the N-S equation. The flow turbulence model is chosen the *SST k-ω*.

2.1 Physical model and boundary conditions

The physical model of the coupled final stage is developed by taking a 300 MW turbine as the research object and considering the influence of the final stage on the flow field of the exhaust passage [16, 17]. Therefore, a physical model of the full-size exhaust passage of the coupled final stage is established. The exhaust passage is mainly composed of the exhaust cylinder and the throat of the condenser. The exhaust cylinder is mainly composed of the diffuser, the worm shell, the reinforcement bars, and the reinforcement plates. The diffuser is mainly composed of the guide ring and the guide cone. The cone is not a center-symmetric structure, and its starting diffusion angle is 15° when the flow line and cone fit best. Since the low-pressure cylinder is a symmetrical structure, and other structures in the passage have less influence on the aerodynamic performance of the exhaust passage, half of the exhaust cylinder is selected as the calculation area in this paper to reduce the calculation volume and improve the calculation efficiency. The simplified model of the exhaust passage is shown in Fig. 1c, and the model of the final stage blade is shown in Fig. 1d. The final stage blade parameters are shown in Table 2, including 52 static blades, 80 rotor blades, a static blade height of 959 mm, a rotor blade height of 1029 mm, and the axial clearance between the rotor and static blades of 111.5 mm.

Table 2 Main parameters of the last stage blades

Item	Value
Height of stator blades	959 mm
Height of rotor blades	1029 mm
Rotation Speed	3000 r/min
Number of stator blades	52
Number of rotor blades	80
Axial distance	2 mm

The grid of the calculation model adopts a combination of structured and unstructured grids, using Turbo-Grid to divide the structured grid of the final blade grid basin into hexahedral grids and applying ICEM to divide the unstructured grid of the whole exhaust passage basin. The topology of rotor and static blade grids is the "HOH" structure, and the "H" orthogonal grid is used for blade inlet and outlet sections. The mesh at the intersection of the final stage rotor and static blades, the intersection of the final stage rotor blades and the inlet of the exhaust passage, and the area near the wall is locally encrypted to achieve a more realistic transfer of flow parameters at the rotor-static intersection. The grid of the computational domain of the exhaust passage and the final stage blades is shown in Fig. 2e and f. In this paper, 100% turbine heat acceptance (THA) is used as the benchmark. The so-called heat consumption acceptance condition is the power issued by the turbine under the rated steam inlet parameters, rated back pressure, normal operation of the heat return system, and zero make-up water rate for continuous operation. This condition is the acceptance condition for the guaranteed value of the heat consumption rate. The irrelevance of the grid was verified for the fluid domain at 100% THA, as shown in Fig. 1g. The physical model is divided into different number of meshes and simulated numerically. The simulation results are analysed for the outlet pressure and velocity of the exhaust channel. It can be seen that when the grid reaches about 7.75 million,
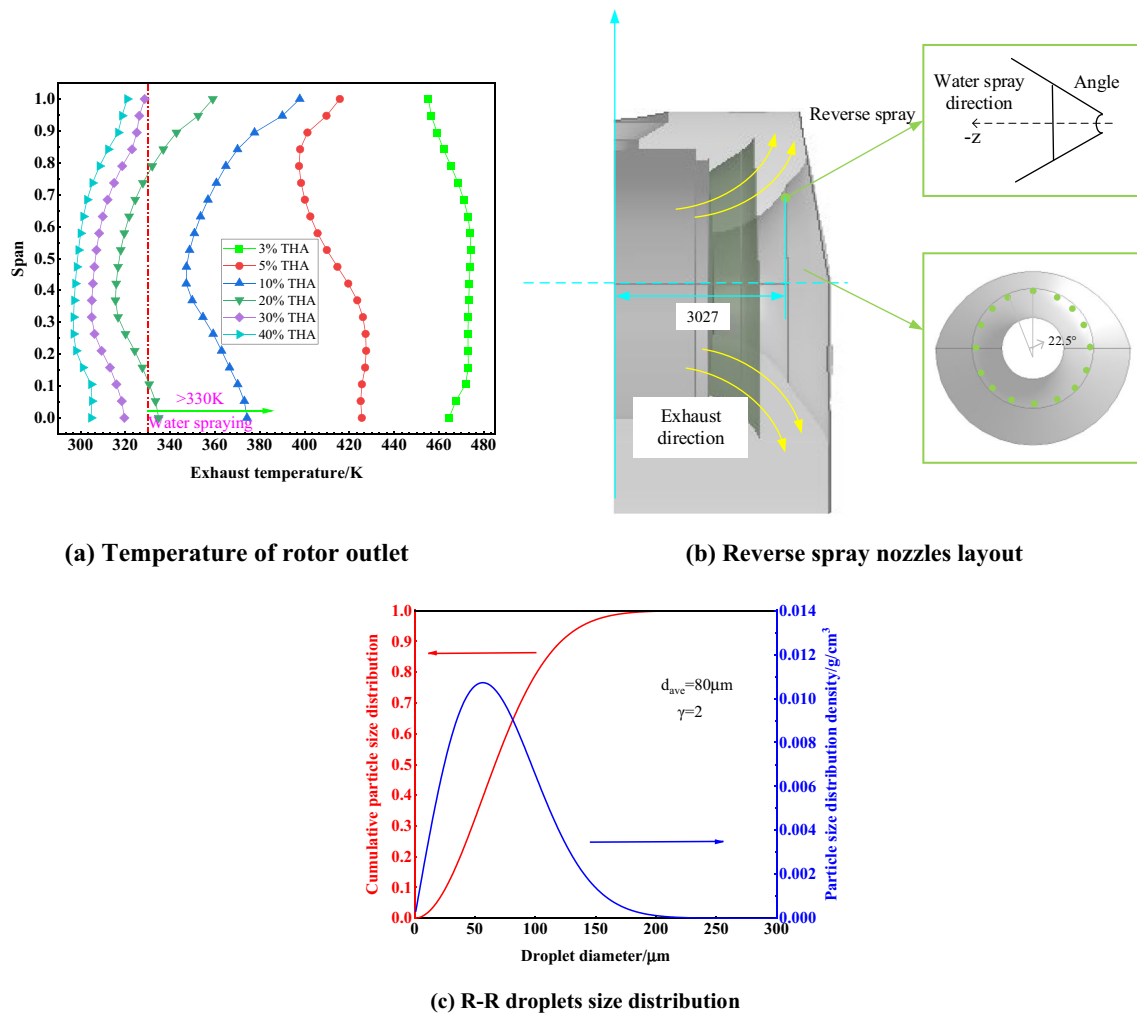

(a) Temperature of rotor outlet

(b) Reverse spray nozzles layout

(c) R-R droplets size distribution

Fig. 2 **a** Temperature of rotor outlet. **b** Reverse spray nozzles layout. **c** R-R droplets size distribution

the exhaust passage outlet pressure and the velocity remain approximately constant. This paper uses a grid number of 7.75 million for the calculation to improve the calculation efficiency and ensure the accuracy of the calculation.

In this paper, the temperature distribution of the final stage rotor vane outlet for six operating conditions is calculated under the low load of the turbine, as shown in Fig. 2a. The leaf root and top temperature have exceeded 330 K under 20% THA condition, and the lower the load, the higher the exhaust temperature. The excessive exhaust temperature will cause a large deformation of the cylinder, which will cause the unit's vibration to exceed the limit and the static and rotor friction accidents [18].

It is necessary to reduce the temperature of the exhaust passage by spraying water to avoid the phenomenon of over-temperature in the exhaust passage. The cooling water mainly comes from condensate, which ensures the water source's cleanliness but can also achieve a good cooling effect. The new water jet device proposed in this paper is a uniform arrangement of water jets on the wall of the cone of inflow, and the direction of this jet is opposite to the direction of exhaust flow, i.e., reverse jet, as shown in Fig. 2b. This water jet is set up with 16 water jets, the angle between the two jets is 22.5°, and the nozzle angle is 60°.

The inlet boundary condition is mass flow rate, given the total inlet temperature and mass flow rate, and the outlet boundary condition is pressure, setting the pressure at the throat outlet to a constant value and the average static pressure to 4900 Pa. The boundary conditions for the 100% THA condition are shown in Table 3. The total inlet temperature for the other conditions is calculated according to the detailed variable condition procedure for small-volume flow.

The rotor blade basin is a rotating domain with a speed of 3000 r/min. The static vane and the exhaust passage are set in the stationary domain. No-slip, adiabatic wall conditions are used, the rotor-static intersection is a hybrid plane method, and the differential format is a high-precision solution model with a residual convergence accuracy of 10^{-5}. The R-R model simulates the particle diameter distribution ejected from the nozzle to more closely match the initial droplet size distribution from the nozzle in the experimental test with the Rosin–Rammler (R-R) method [19]. The R-R average particle size (d_{ave}) under the initial droplet distribution is calculated as follows:

Table 3 Boundary parameters of 100% THA

Parameters	Values
Inlet total temperature	65.6℃
Inlet mass flow rate	82.167 kg/s
Outlet average static pressure	4900 Pa

$$R = exp\left[-\left(d_p/d_{ave}\right)\right]^{\gamma},\tag{1}$$

where R is the cumulative mass fraction of the diameter lower than d_p of the cumulative mass fraction, γ is the diffusion parameter of particle size dispersion, and d_{ave} is the size of R equal to 1/e. In this paper, the average diameter of water droplets is 80 μm, and the uniformity index is 2. The cumulative particle size distribution and particle size distribution density are given in Fig. 2c.

2.2 Mathematical model

In the process of water spray, the fluid in the exhaust passage includes the exhaust steam of the steam turbine, the cooling water droplets, and the evaporating. Therefore, the multicomponent and multi-phase flow includes water droplets evaporation, heat and mass transfer, and phase change. Due to the process involving discrete and continuous phases, the Euler–Lagrange particle tracking method is applied to investigate the water spray. Although the discrete and continuous phases are modeled separately, their coupling is achieved by introducing mass, momentum, and energy sources.

2.2.1 Water spray model

In this paper, the Eulerian–Lagrangian particle tracking method is applied to study the complex phase change heat and mass transfer process in the water spraying process, which mainly involves the two-phase coupling process of mass, momentum, and heat transfer between continuous and discrete phases [20]. The sprayed droplets are considered the disperse phase, the wet steam contains saturated steam, and the water vapor is set as the continuous phase to properly simulate the droplet/water vapor two-phase flow and evaporative cooling process. Considering the effects of mass, momentum, and heat transfer, the effect of droplets on the continuous phase is taken as the source term of the N-S equation.

Control equation for the continuous phase:

$$\frac{\partial \rho}{\partial t} + \nabla(\rho \vec{u}) = S_m \tag{2}$$

where ρ and $\vec{u}$ are the density and velocity of the wet steam mixture (steam and water), kg/m and m/s, respectively, and S_m is the mass transfer from the discrete phase to the continuous phase.

The conservation of momentum equation for the continuous phase:

$$\frac{\partial}{\partial t}\left(\rho \vec{u}\right) + \nabla\left(\rho \vec{u}\vec{u}\right) = -\nabla \rho + \nabla\left[\overline{\overline{\tau}}\right] + \vec{F}_{ext} \tag{3}$$

The source term, $\vec{F}_{ext}$, is the external force, which is the momentum transfer from the water droplet to the continuous term.

The source term, $\vec{F}_{ext}$, is the external force, which is the momentum transfer from the droplets to the continuous term, N.

Viscous shear stress tensor $\overline{\overline{\tau}}$:

$$\overline{\overline{\tau}} = \mu[(\nabla \vec{u} + \nabla \vec{u}^T) - 2\nabla \cdot \vec{u}I/3] \tag{4}$$

where μ is the rotor viscosity, N—s/m². I is the unit tensor.

The average energy equation for the continuous phase:

$$\frac{\partial}{\partial t}(\rho h_t) + \nabla \cdot \left[\vec{u}(\rho h_t + \rho)\right] = \nabla \cdot (\lambda \nabla T + \overline{\overline{\tau}} \cdot \vec{u}) + \vec{u} \cdot \vec{F} + S_h \tag{5}$$

where h_t is the total enthalpy, J/kg, λ is the thermal conductivity considering turbulence effects, W/(m–K), and S_h denotes the heat transfer between the continuous and discrete phases.

Treating the droplet spray as a discrete phase is a feasible way to simulate spray cooling due to the small volume fraction of the liquid. In the two-phase coupling of droplet evaporation, the droplet will complete the mass, heat, and momentum exchange during the evaporation process [21]. The control equations for the continuous and dispersed phases achieve the interphase exchange of heat, mass, and momentum between the droplet and the continuous phase. The sprayed droplet particles exist in the motion of the wet vapor mixture, and the motion equation of the discrete phase is defined as follows:

$$m_P \frac{d\vec{u}_p}{dt} = \vec{F}_D + \vec{F}_B + \vec{F}_T + \vec{F}_{VM} + \vec{F}_P + \vec{F}_R + \vec{F}_{BA} \tag{6}$$

where m_P is the water droplet mass, kg. $\vec{u}_p$ is the water droplet velocity, m/s. $\vec{F}_D$ is the drag force of the steam acting on the water droplet, N. $\vec{F}_B$ is the water droplet buoyancy, N. $\vec{F}_T$ is the turbulent dispersion force, N. $\vec{F}_{VM}$ is the virtual mass force, N. $\vec{F}_P$ is the pressure gradient force, N. $\vec{F}_R$ is the force due to domain rotation, N. $\vec{F}_{BA}$ is the Basset force, N.

Pressure gradient force $\vec{F}_P$ is not considered because the water droplet density is bigger than the steam density in this paper. Since the density ratio of the steam to the water droplet is less than 0.002, the effect of $\vec{F}_{BA}$ can be neglected too [22].

The rate of temperature change of the particle can be found by the following equation [23]:

$$m_p C_{p,w} \frac{dT_p}{dt} = \pi d_p \lambda_w Nu(T - T_p) + h_{lh}\frac{dm_p}{dt} \tag{7}$$

where $C_{p,w}$ is the specific heat of the water droplet, J/(kg-°C), d_p and T_p are the particle size and temperature of the water droplet, μm and °C, respectively, λ_w is the thermal conductivity of wet vapor, W/(m–K), and Nu is the Nusser number to evaluate the heat transfer of water vapor/droplet.

The process can be divided into forced convection evaporation in the boiling state and natural convection evaporation in the non-saturated state because temperature and pressure affect particle evaporation. The saturation pressure can be estimated from the Antoine equation [24]:

$$\log_{10}p_{sat} = A - \frac{B}{(T + C - 273.15)} \tag{8}$$

where the Antoni reference state constant A is 11.779, the Antoni enthalpy coefficient B is 3885.704, and the Antoni temperature excursion constant C is 230.23 K.

Depending on whether the temperature of the droplet is above or below the boiling point, there are two ways to solve for the mass transfer rate according to the Antoine equation in this model, which is governed by the following factors in the boiling state:

$$\frac{d_{mp}}{d_t} = -\pi d_p \lambda Nu \frac{(T - T_p)}{h_{ih}} \tag{9}$$

In the unsaturated state, the mass transfer rate can be obtained from the following expression:

$$\frac{d_{mp}}{d_t} = \pi d_p \rho_{wv} Sh \frac{M_{wv}}{M} \log\left(\frac{1 - f_p}{1 - f}\right) \tag{10}$$

where ρ_{wv} and D_{wv} are the density and diffusivity of water vapor in kg/m and m s²ᐟ, M is the molar mass of wet vapor in g/mol, M_{mv} is the molar mass in water vapor in g/mol, f_p and f are the molar fractions of liquid droplets and wet vapor, respectively, that can be used to evaluate the Sherwood number of wet vapor/droplet mass transfer. Parameter Sh can be calculated by the following equation:

$$Sh = 2 + 0.6Re^{1/2}(\frac{\mu}{\rho_{wv}D_{wv}})^{1/3} \tag{11}$$

where Re is the similar criterion number Reynolds number that characterizes the effect of viscosity in fluid mechanics.

2.2.2 Turbulence model

The flow in the exhaust passage is mainly turbulent, with a very complex vortex system structure in the cylinder. The flow turbulence model *SST k-ω* is chosen to consider the effect of the shear stress model and simulate the turbulent motion in the exhaust passage, which can meet the needs of the complex flow in the exhaust passage under small volume flow [25]. The *SST k-ω* model is as follows:

$$\frac{\partial(\rho k)}{\partial t} + \frac{\partial(\rho k u_i)}{\partial x_i} = \frac{\partial}{\partial x_j}(\Gamma_k \frac{\partial k}{\partial x_j}) + \widetilde{G}_k - T_k + S_k \tag{12}$$

$$\frac{\partial(\rho\omega)}{\partial t} + \frac{\partial(\rho\omega u_i)}{\partial x_i} = \frac{\partial}{\partial x_j}(\Gamma_w\frac{\partial w}{\partial x_j}) + G_w - Y_w + D_w + S_w$$

(13)

$$\mu_t = G_w\rho\frac{k}{\omega}$$

(14)

where G_k and Gw are the generating terms of turbulent kinetic energy k and dissipation rate ω, respectively, Γ_k and Γ_ω are the effective diffusion coefficients of k and ω, respectively, Y_k and Y_ω are the dissipation of k and ω caused by turbulence, respectively, D_ω is the cross-diffusion term, and S_k and $S\omega$ are the source terms.

2.3 Validation

Sureshkumar et al. [8] conducted an experimental study of water jet cooling in a wind tunnel experiment with a water jet cooling device similar to the operating and geometric conditions simulated in this paper. The wind tunnel in the experiment has a length of 1.9 m and a cross-section of 0.585 m * 0.585 m. Nine pairs of thermocouples are distributed at the outlet, and each pair measures the dry bulb temperature (DBT) and the wet bulb temperature (WBT), respectively. In this paper, the above numerical simulation method was used to calculate the experimental data of a set of DBTs. The simulated model, i.e., the monitoring point, is shown in Fig. 3a. The boundary conditions are the inlet wind speed of 1 m/s and DBT of 41.4℃. The water spray system is a hollow cone nozzle with a diameter of 4 mm, a cone angle of 22°, and a pressure of 3 bar. Figure 3b shows the comparison of DBT with the numerical solution. It can be seen that the relative errors of the numerical solutions are within ± 5%, proving that the numerical model established in this paper is reliable and feasible.
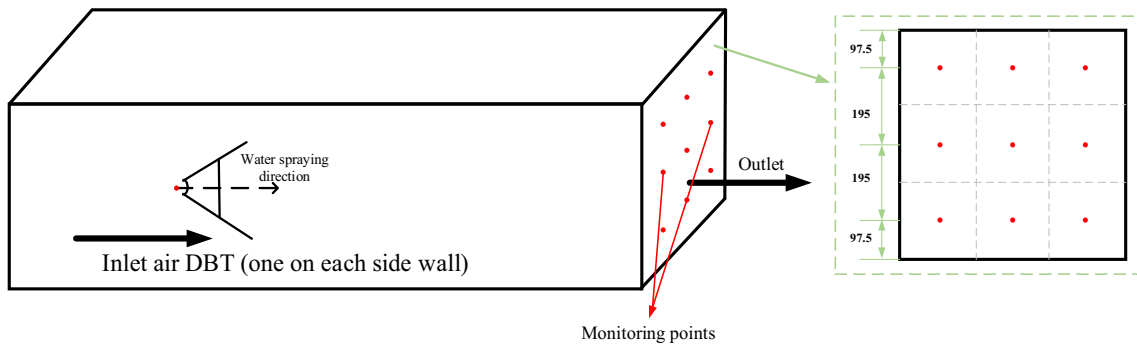
(a) Physical model and monitoring point of validation
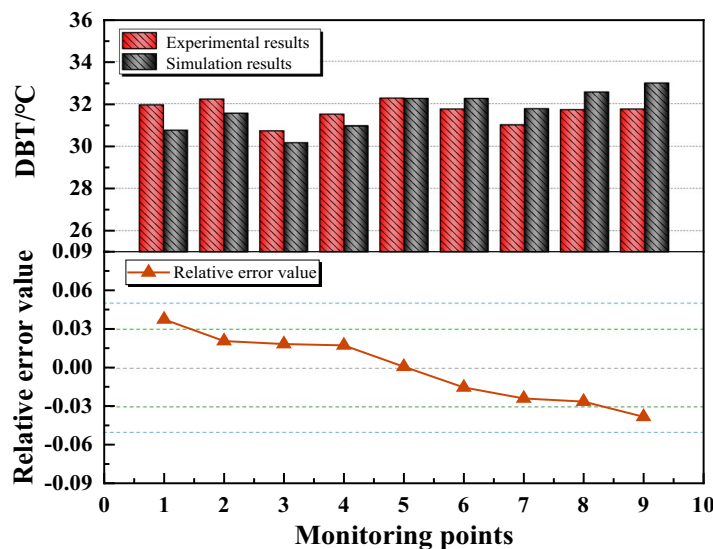
(b) Error analysis of experiment results and simulation results

Fig. 3 Experimental verification of nozzles

3 Calculation results and discussion

Because of the water spray, the velocity and temperature distribution are uneven in the exhaust passage. Therefore, the variation between the water spray volume and evaporation volume is analyzed first. Meanwhile, the cooling effect of water spray is analyzed during windage.

3.1 Water spraying volume and evaporation

Figure 4a gives the relationship between the temperature of the exhaust steam and the load when the water is not sprayed. Figure 4a shows that as the load decreases, the blowing situation becomes more and more serious. The frictional heat the blowing generates increases, and the exhaust steam temperature rises. The amount of water spray must be increased to bring the exhaust steam temperature down to a reasonable range. At the same time, the amount of water sprayed under different loads is given in Fig. 4a. For quantitative comparison, the amount of water sprayed is the same for both downward and reverse spraying. Figure 4b shows the same simulation process under the same working conditions, amount of water spray, and reverse and forward spray water evaporation. From the Fig., it can be seen that the evaporation volume increases as the load is reduced. This is due to the temperature of the temperature reduction water being certain; the higher the temperature of the exhaust steam, the greater the temperature difference between the two, the greater the power of heat transfer, the more liquid water vaporization, the greater the evaporation rate, and therefore the greater the evaporation amount. A comparison of the two types of water spraying can be seen. The evaporation of reverse spraying is greater than the evaporation of forward spraying in the case of other conditions that are the same.

On the one hand, reverse spraying is when the temperature reduction of water and incoming steam are in opposite directions. Hence, the temperature reduction of water and incoming steam hit each other. The joint impact force will strengthen the convective heat transfer between liquid droplets and steam, accelerating the evaporation rate of liquid droplets. On the other hand, compared with reverse spraying and downward spraying, the droplets stay in the exhaust passage for a long time, the droplets and steam heat exchange time is long, and the droplet evaporation volume is large.

3.2 The effect of the water spraying method on the flow field of the exhaust passage

Figure 5 gives the flow diagrams of the exhaust passages under different loads, without water spraying, with spraying, and against spraying in three cases. As seen from Fig. 5a, both passage and backflow vortices are in the diffuser at a small volume flow rate.

When the steam passes through the small space above the volute passage, the volume decreases, and the density increases, forming passage vortices. The passage vortices affect the steam flow until the outlet of the condenser throat. Under low load, besides the passage vortices, the exhaust steam forms the reverse vortices in the diffuser passage. There are two different vortices in the left and right mid-horizontal plane due to two different vortices in the left and right mid-horizontal plane. This can be attributed to the inlet steam of the exhaust passage not being symmetrical in the circumferential direction.
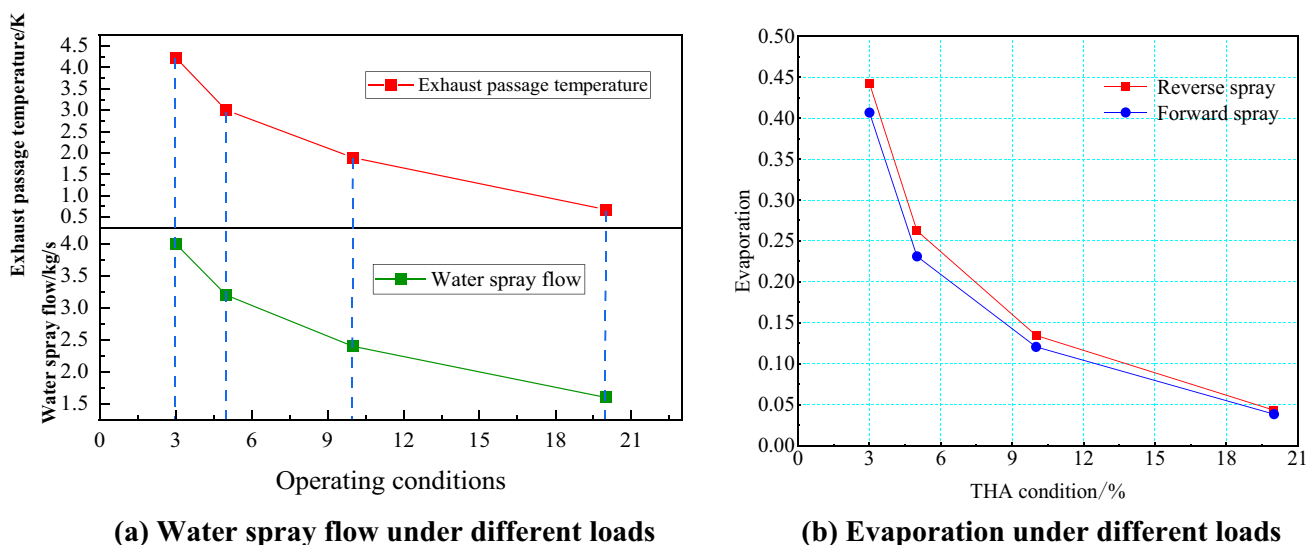

(a) Water spray flow under different loads

(b) Evaporation under different loads

Fig. 4 **a** Water spray flow under different loads. **b** Evaporation under different loads

(a) No water spraying

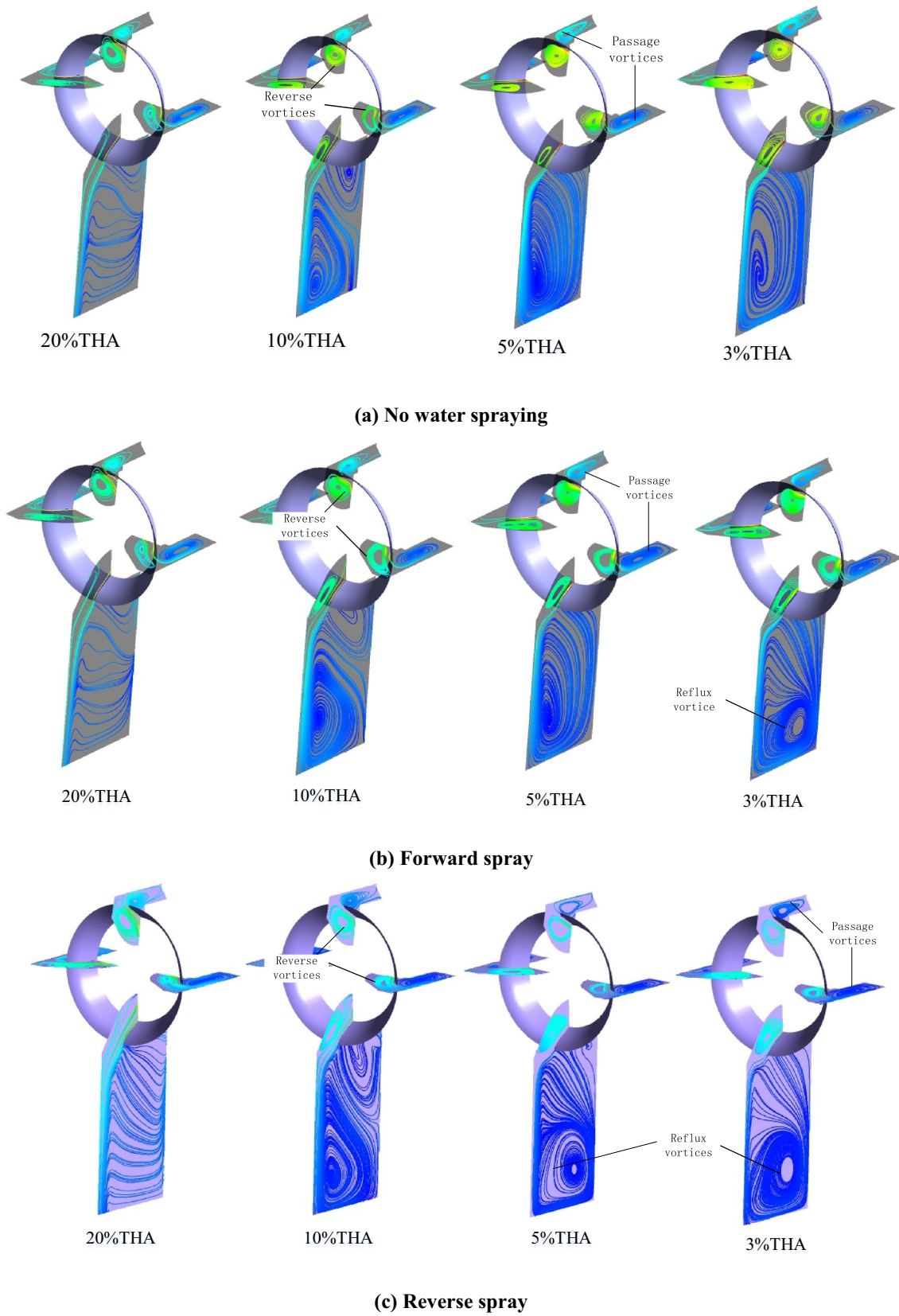**(b) Forward spray**

(c) Reverse spray

Fig. 5 Flow streamlines of exhaust passages under different conditions

With the flow rate decreasing, the reverse flow area gradually increases, and the low-velocity steam fills the entire diffuser passage, so the ability to overcome the flow resistance decreases. After spraying water, the evaporation of temperature-reduction water into steam increases the reel-suction effect of the return flow, especially increasing the outlet return area of the exhaust passage (Fig. 5b, c). In reverse spraying, the small droplets ejected from the nozzle and the direction of the flow of exhaust steam in the opposite direction, increasing the collision and rotation, the formation of a strong vortex, sucking the surrounding vapor flow, and forming a larger reflux area. The lower the load, the more water is sprayed, and the larger the reflux area c.

3.3 The effect of water spraying on the aerodynamic performance of the exhaust passage

Figure 6A shows the pressure distribution cloud on the wall of the cone before water spraying under 20% THA conditions. Figure 6A1, A2, A3 and A4 show the corresponding pressure distribution curves at four positions along the steam inlet direction under different conditions. The horizontal coordinates of the graph are the dimensionless arc length clockwise along the wall of the cone, and the starting point is the intersection point with the cone wall in the XY plane of the cone in the positive direction of the X axis. After the spray water, the pressure increased but did not change the pressure along the circumferential trend of the cone.

The change in pressure can be seen from A1 and A2 two curves. The pressure increase in the reverse spraying is greater than the pressure increase in the forward spraying, and in 20% THA, 10% THA, 5% THA, and 3% THA under the four operating conditions than the forward spraying pressure increase of about 150 Pa. According to Fig. 6A3, reverse spraying A3 curve fluctuations are relatively large, which is because the reverse spraying of the water jet in A3 Near the curve, the spraying of water on the pressure near the spray nozzle is obvious, and the spraying angle is 60°. Consequently, the A3 curve at different locations by the droplet impact force is also different, so the pressure fluctuations near the A3 curve are obvious. However, in the vicinity of the A4 curve, the pressure is the same in the three cases of unsprayed water, reverse spraying, and smooth spraying. According to different working conditions, A1, A2, A3, and A4 pressure changes on these four curves can show that water spraying on the pressure after the water jet has no effect.

A comparative analysis of the static pressure recovery capacity and the flow loss of the vapor stream under different loads was conducted for three cases to quantitatively evaluate the effect of water spraying on the aerodynamic performance of the exhaust passage. The hydrostatic pressure recovery reflects the hydrostatic pressure recovery coefficient C_p, and the flow loss of the vapor stream is reflected by the total pressure drop Δp in the exhaust passage. The static pressure recovery coefficient C_p is defined in Eq. (15), and the total pressure drop Δp is defined in Eq. (16):

$$C_p = \frac{p_{s,out} - p_{s,in}}{p_{t,in} - p_{s,in}} \tag{15}$$

where $p_{s,in}$ and $p_{s,out}$ are the mass-averaged static pressures at the inlet and outlet of the exhaust passage, Pa, respectively, and $p_{t,in}$ is the mass-averaged total pressure at the inlet of the exhaust passage, Pa.

$$\Delta p = p_{t,in} - p_{t,out} \tag{16}$$

where $p_{t,in}$, $p_{t,out}$ are the mass-averaged total pressure at the inlet and outlet of the exhaust passage, respectively, Pa.

Figure 7a shows the hydrostatic recovery coefficients for different operating conditions. It can be seen that as the mass flow rate decreases, the hydrostatic recovery coefficient decreases in all three cases. In other words, as the mass flow rate decreases, the kinetic energy of the vapor flow in the exhaust passage becomes less capable of being converted into hydrostatic energy. The aerodynamic performance worsens, and the economy of the turbine becomes worse. In addition, it can be seen that the hydrostatic pressure recovery coefficient becomes smaller after water spraying than before, indicating that water spraying worsens the aerodynamic performance of the exhaust passage.

Furthermore, compared to the forward spraying, the static pressure recovery coefficient of the reverse spraying is smaller, with a maximum reduction of 8.17%, Since the direction of the water droplets ejected during the reverse spray and the flow of steam in the exhaust channel are opposite, there will be an impact on the incoming flow of steam, making the flow field of steam more turbulent and increasing dissipation losses. In addition, due to the impact after the reduction in the velocity of steam flow, the expansion function of the pressure expansion structure of an exhaust channel is also reduced. The combined effect of the two will make the static pressure recovery coefficient smaller.

The total pressure drop in the discharge channel can reflect the flow loss of the vapor stream, as shown in Fig. 7b. The total pressure drop in the exhaust channel becomes larger after water spraying, and it is larger when spraying against than when spraying with. The pressure drop of steam flow from the entrance to the exit of the exhaust channel contains two parts, partly due to the high degree of turbulence within the steam flow. The degree of turbulence and serious energy dissipation reduces the speed and pressure. The other part is that the exhaust cylinder "horn" structure has the function of pressure expansion to reduce the speed and pressure increase. The total pressure drop of the exhaust channel is the interaction of
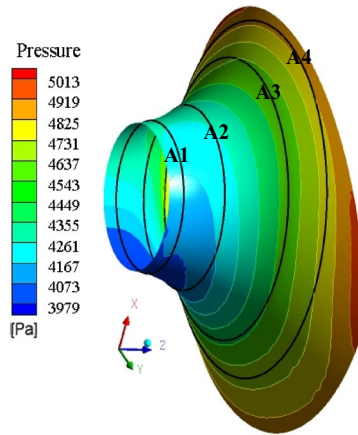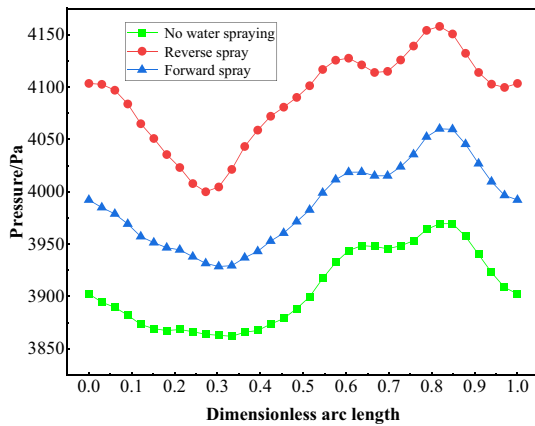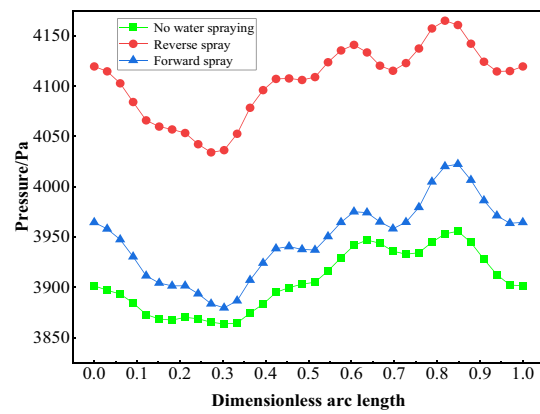
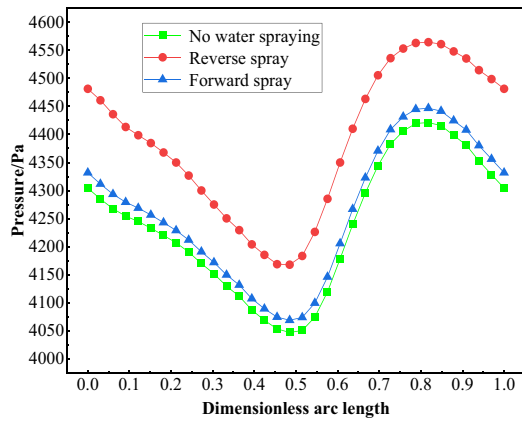**(A)Pressure distribution on guide cone wall**
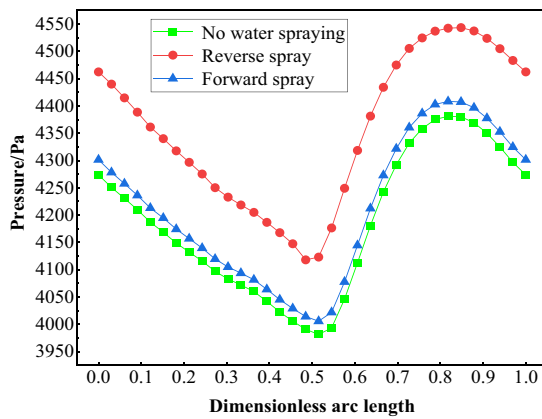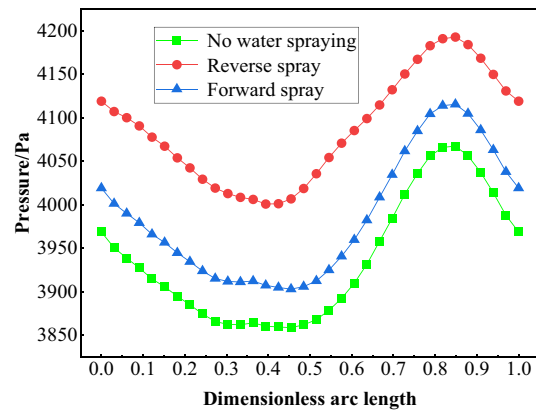
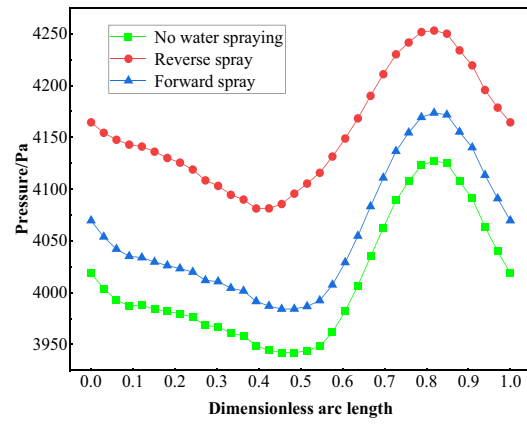(A1a)20%THA

(A1b)10%THA

(A1c)5%THA

(A1d)3%THA

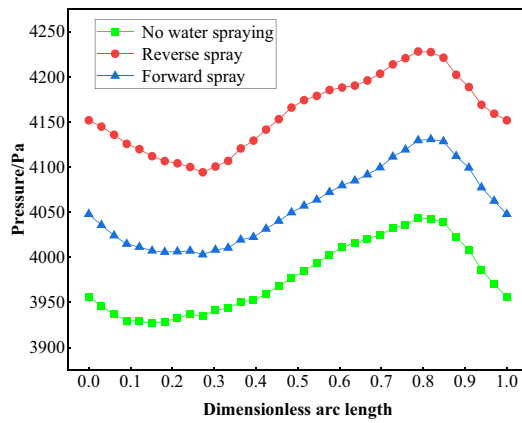**(A1) pressure under different conditions**

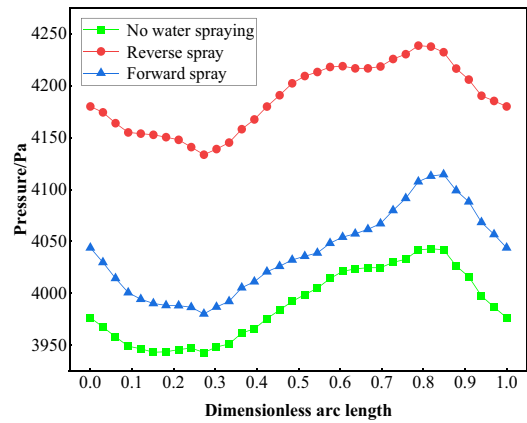**Fig. 6** Note: This data is mandatory. Please provide
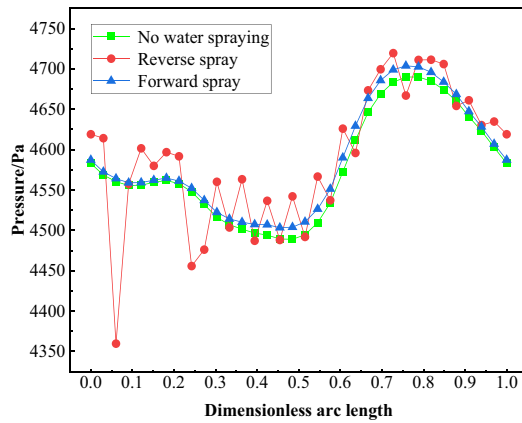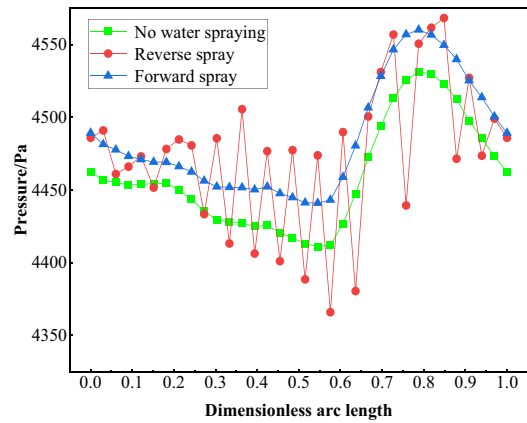
(A2a)20%THA

(A2b)10%THA
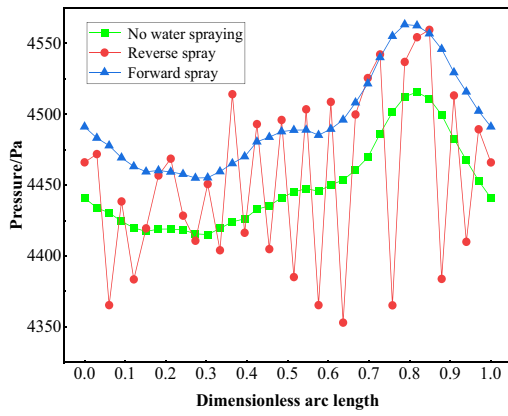
(A2c)5%THA

(A2d)3%THA

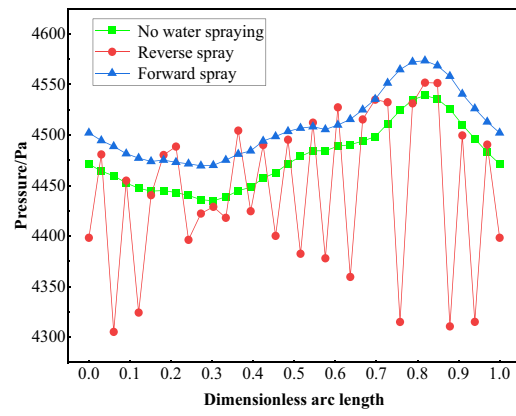**(A2) pressure under different conditions**
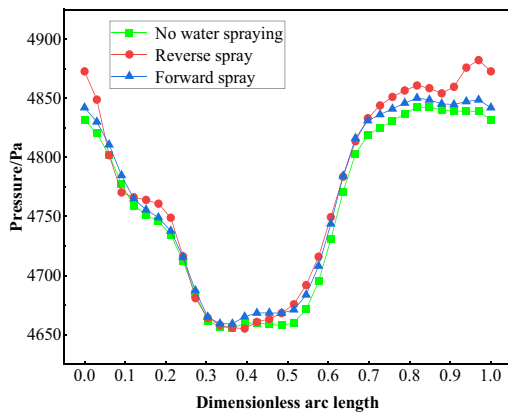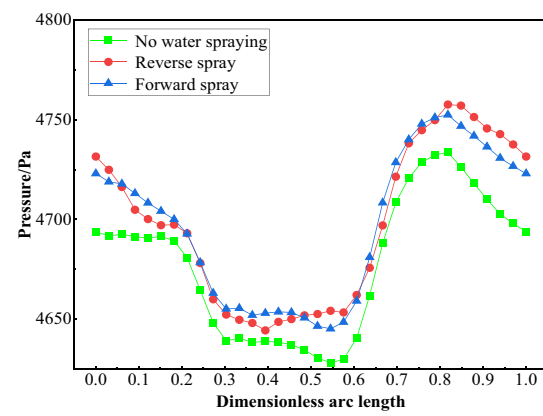
(A3a)20%THA

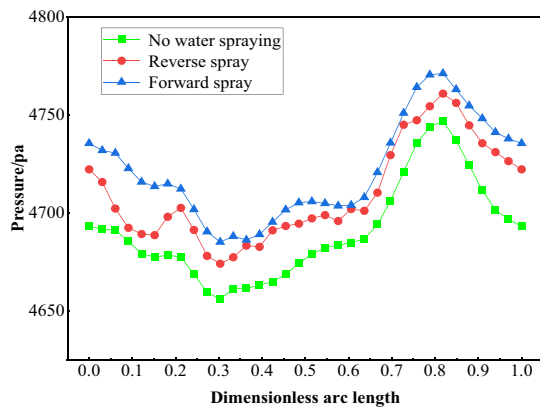(A3b)10%THA

Fig. 6 (continued)
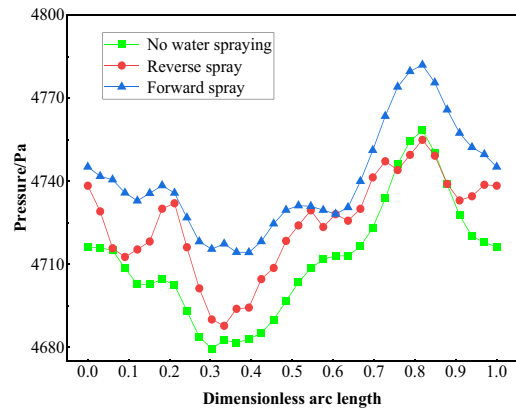
(A3c)5%THA

(A3d)3%THA

(A3) pressure under different conditions

(A4a)20%THA

(A4b)10%THA

(A4c)5%THA

(A4d)3%THA

(A4) pressure under different conditions

Fig. 6 (continued)

(a) C_p **under different conditions**

(b)Total pressure drop Δp under different conditions

(c) λ_v **under different conditions**
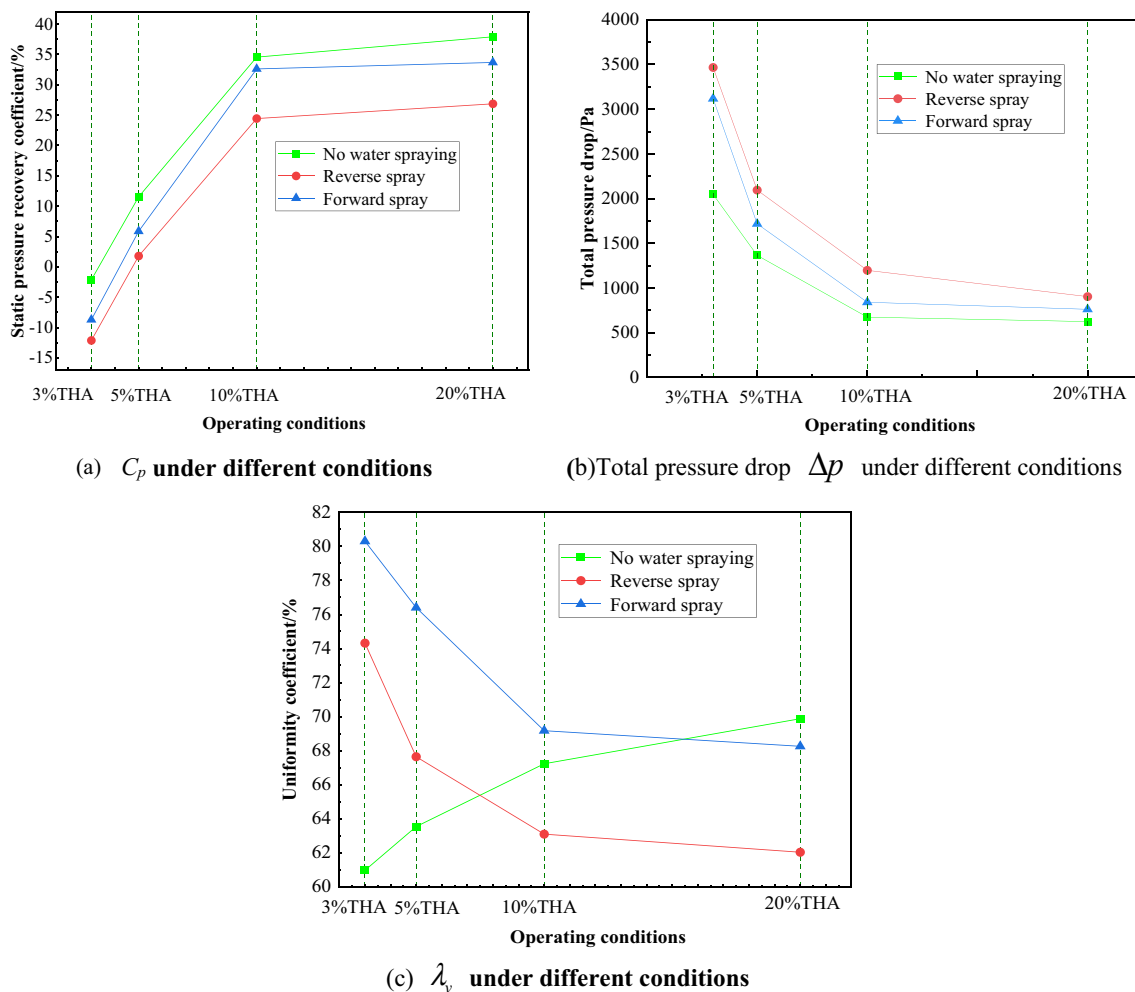
Fig. 7 **a** C_p under different conditions. **b** Total pressure drop Δp under different conditions. **c** Total pressure drop Δp under different conditions

these two because the steam flow in the exhaust cylinder is spiral flow. Internal dissipation losses accounted for a larger proportion, so the steam flow shows the pressure drop phenomenon. After water spraying, the sprayed water droplets make the flow field of steam more turbulent, and the dissipation loss becomes larger. In addition, after water spraying, the flow speed decreases, and the pressure expansion function of the exhaust cylinder is weakened. Compared with the downstream spraying, the total pressure drop of the reverse spraying is greater, mainly because the impact of the reverse spraying increases the mixing and dissipation losses, resulting in a greater total pressure drop.

The exit velocity uniformity coefficient reflects the influence of the upstream inflow on the forward. The larger the uniformity coefficient, the more uniform the exit flow, and the better the heat transfer effect of the condenser. The uniformity coefficient of the outlet velocity at the throat can be defined as:

$$\lambda = \left(1 - \frac{V_m - V_a}{V_m}\right) \times 100\% = \frac{V_a}{V_m} \times 100\% \qquad (17)$$

where V_a and V_m are the area-averaged velocity and mass-averaged velocity, m/s, respectively.

As can be seen in Fig. 7c, the uniformity coefficient decreases as the mass flow rate decreases when the water is not sprayed. However, after the water is sprayed, the uniformity coefficient becomes larger as the mass flow rate decreases, and the uniformity coefficient when the reverse spray is smaller than the uniformity coefficient when the downward spray is applied. The small droplets ejected from the nozzle will be heat exchanged with steam in the exhaust passage and then evaporate into water vapor, which to some extent, is equivalent to an increase in load, which will make the uniformity coefficient larger. However, simultaneously, the sprayed droplets will also produce a certain amount of interference with the flow field so that the flow field becomes turbulent, decreasing the uniformity coefficient. Therefore,

the change in uniformity coefficient after spraying water results from the joint action of these two.

In 20% THA conditions, since the amount of water sprayed as well as the evaporation rate are low, the increase in steam flow in the exhaust passage is small, while the small droplets of water ejected from the water jet to produce some interference with the flow field, making the flow field more turbulent. Therefore, the uniformity coefficient becomes smaller after spraying water than before. In the 10% THA conditions, the uniformity coefficient is the largest when spraying forward, while the uniformity coefficient is the smallest when spraying upstream. The main reason is that the impact of small droplets ejected from the nozzle on the flow field is smaller than the increase in steam in the exhaust passage, while the reverse is the case. In the two conditions of 3% THA and 5% THA, the uniformity coefficient increases after spraying water compared to before, mainly because the amount of water sprayed under these two conditions increases. Consequently, the amount of evaporation increases, and the amount of steam in the exhaust passage increases, to some extent equivalent to the increase in load. The effect of the increased load is greater than the droplet interference with the flow field, so the uniformity coefficient increases. However, at this time, the uniformity coefficient of the reverse spray is lower than that of the forward spray because the spray volume of the reverse spray is large, the droplet disturbance of the flow field is large, and the uniformity coefficient decreases.

3.4 The effect of water spray on the cooling effect of the exhaust passage

The cooling effect is an important indicator of water jet temperature reduction. The effect of water spraying on the blade temperature is explored by analyzing the temperature clouds on the inlet surface of the exhaust passage. Moreover, four dimensionless curves were taken on the guide cone to analyze the temperature variation on the curves and obtain the effect of water spraying on the cooling effect of the turbine exhaust passage.

3.4.1 The effect of water spray on the temperature of the inlet surface of the exhaust passage

Figure 8 shows the temperature distribution of the exhaust passage inlet under different operating conditions with no water spraying, downward spraying, and reverse spraying. The temperature of the exhaust passage inlet is asymmetrically distributed in the circumferential direction. Under low load, this asymmetry is because although the exhaust passage's inlet shape is symmetrical, the exhaust steam enters the exhaust passage at a certain swirl angle. The

swirl angles are different in the circumferential direction and under different loads.

Without water spraying, the inlet temperature gradually rises as the load decreases. The highest temperature difference between 20% THA and 3% THA conditions can be 100 K. Without water spraying, the highest temperature at the inlet surface of the 20% THA and 10% THA exhaust passages appears in the area adjacent to the top of the leaf. In comparison, at 5% THA and 3% THA, the highest temperature appears at the root of the leaf. This indicates that the leaf root temperature exceeds the maximum leaf temperature, shifting the highest temperature region. The cooling effect of reverse spraying is significantly better than that of down spraying, mainly in the leaf root region. In the 20% THA, 10% THA, 5% THA, and 3% THA conditions, the temperature of the reverse spray cooling than the cooling temperature of the forward spray 12 K, 34 K, 42 K, and 55 K. Reverse spray droplet flow direction and the opposite direction of the flow of steam.

In contrast, with the small volume flow rate under the return vortex, steam on the spray droplets will have a roll suction effect, so the temperature of the inlet surface is relatively low. While in the downward spray, the flow direction of fine droplets and the steam flow direction are the same. Only a small part of the droplets will be surrounded by fluid sucking most of the steam out of the exhaust passage. Lastly, the inlet cooling effect is the worst.

3.4.2 Influence of water spraying method on the temperature distribution on the wall of the inflow ring

Figure 9A shows the temperature distribution cloud on the wall of the cone before water spraying under 20% THA conditions. Figure 9A1, A2, A3 and A4 show the corresponding temperature distribution curves at four locations along the steam inlet direction under different conditions. The horizontal coordinates of the graph are the dimensionless arc length of one week clockwise along the wall of the cone. The starting point is the intersection point with the cone wall in the XY plane of the cone in the positive direction of the X-axis. Four positions, B1, B2, B3, and B4, demonstrate temperature distribution, and the following basic trend is presented:

1. Not sprayed with water when the load decreases,
2. The steam temperature becomes higher,
3. The temperature drops significantly after the spraying, and
4. The temperature drops significantly when the reverse spraying than when the downward spraying.

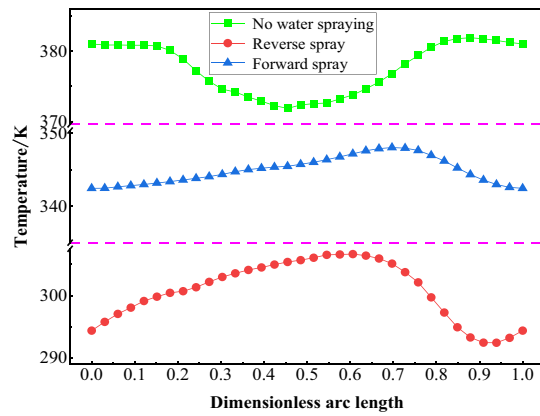**Fig. 8** Temperature Cloud diagram under different conditions
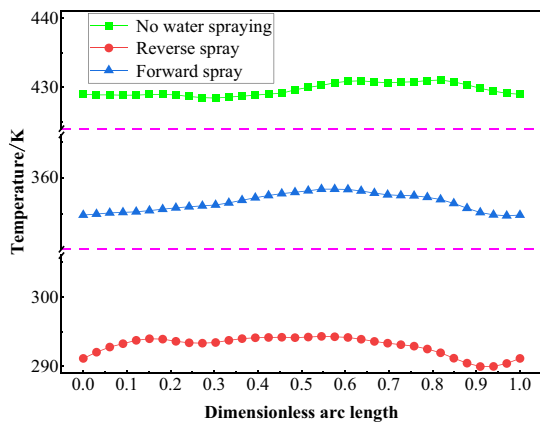

(a)20%THA
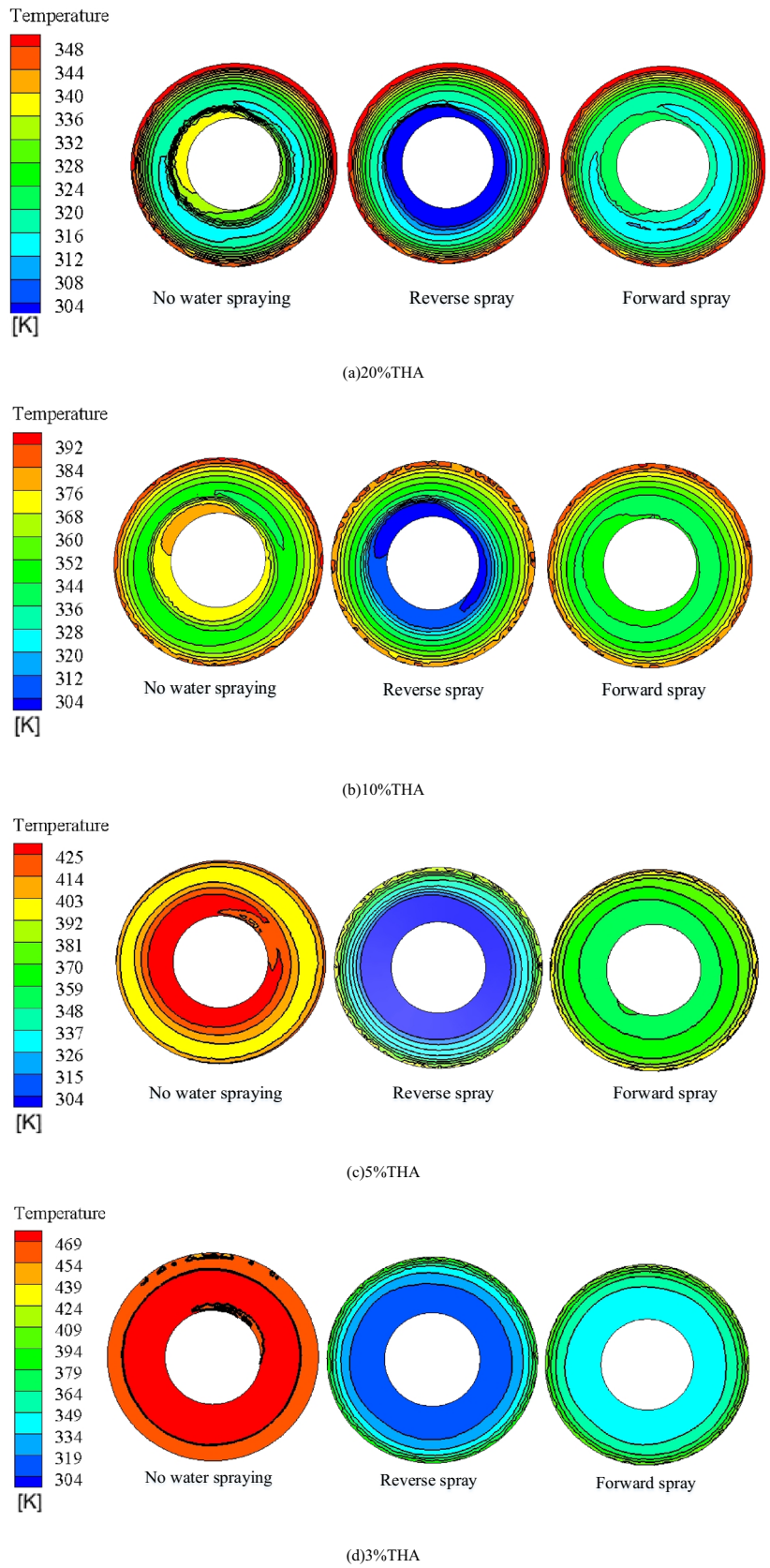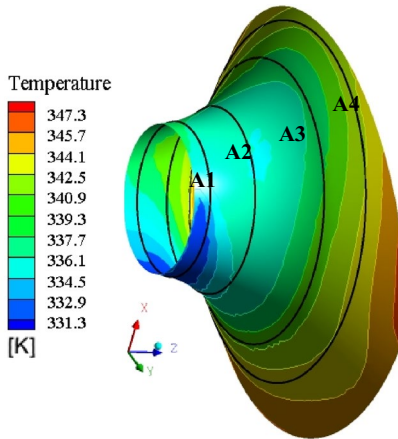
(b)10%THA

(c)5%THA

(d)3%THA

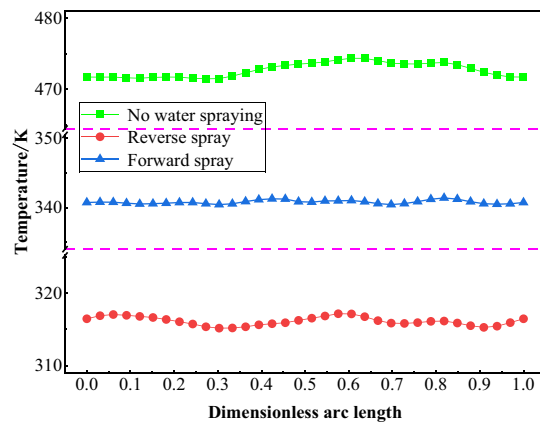**(A) Temperature distribution on guide cone wall**
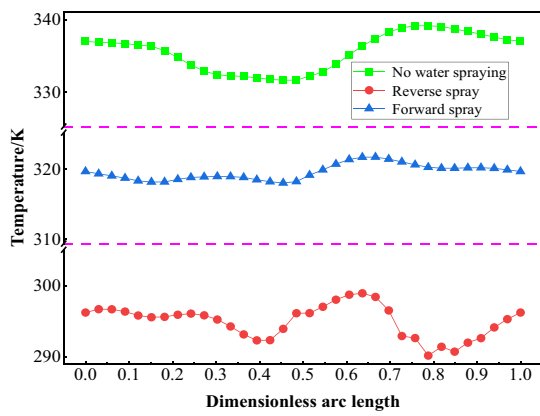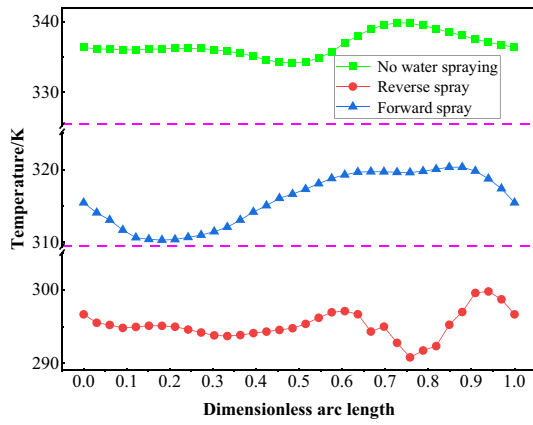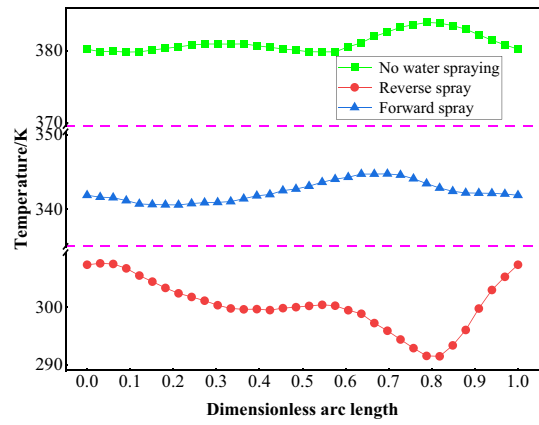

(A1a)20%THA

(A1b)10%THA

(A1c)5%THA

(A1d)3%THA

(A1) temperature under different conditions
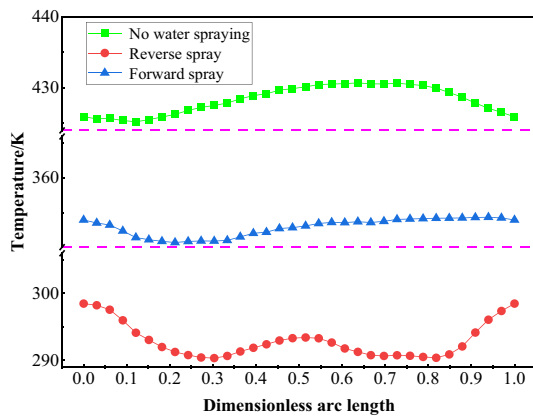
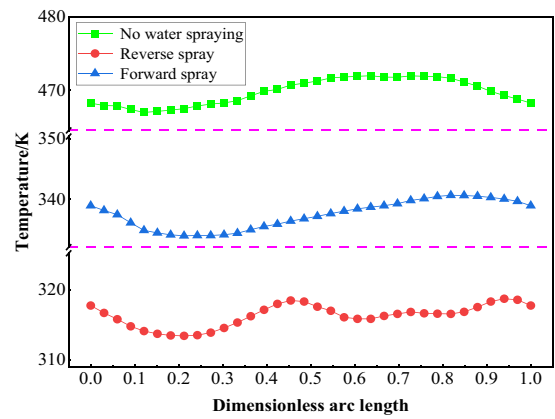**Fig. 9** Note: This data is mandatory. Please provide
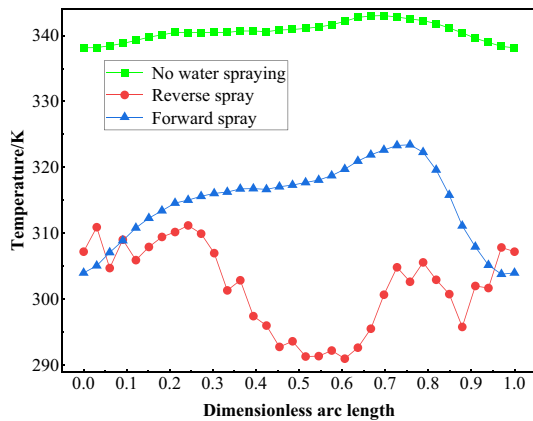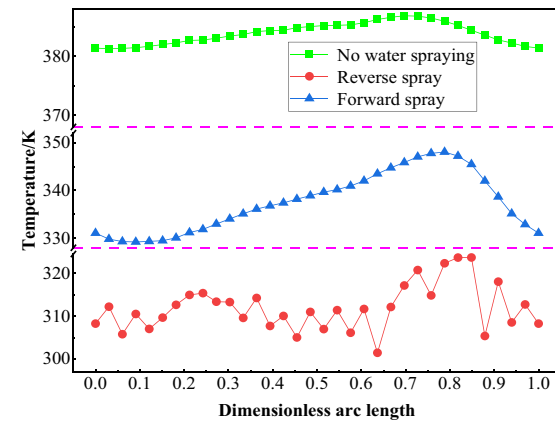
(A2a)20%THA

(A2b)10%THA

(A2c)5%THA
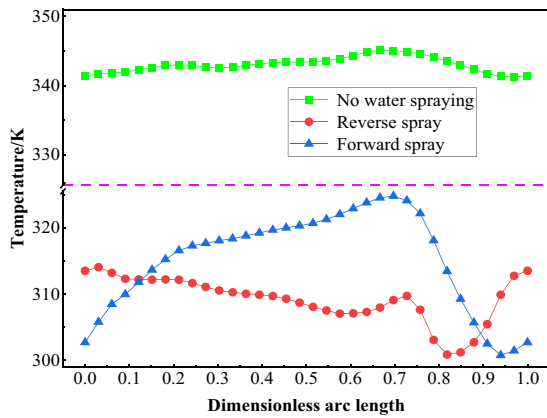
(A2d)3%THA

(A2) temperature under different conditions

(A3a)20%THA
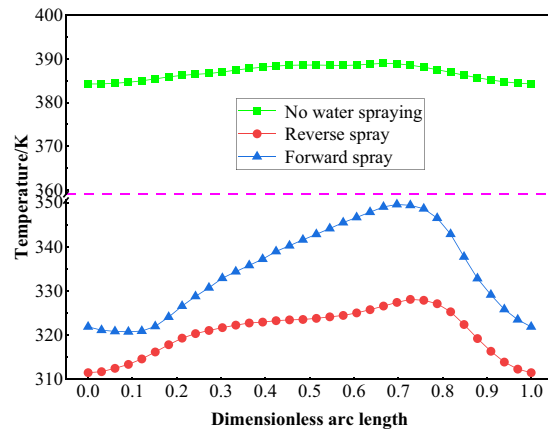
(A3b)10%THA
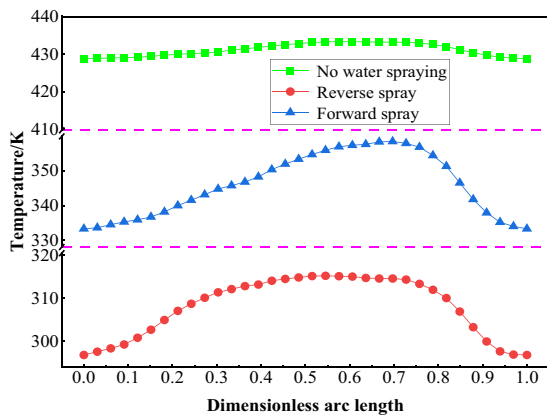
Fig. 9 (continued)
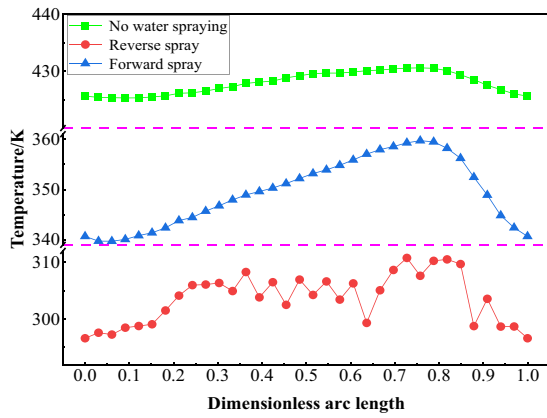
(A3c)5%THA
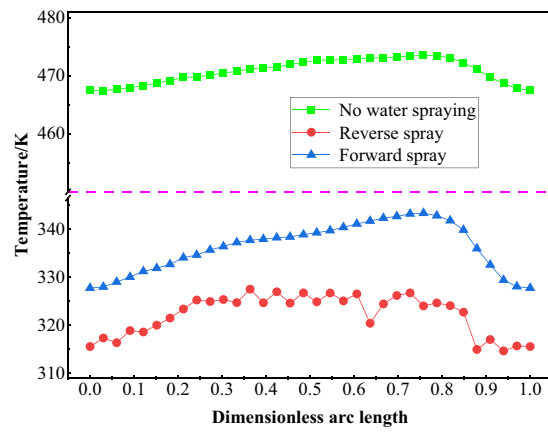
(A3d)3%THA

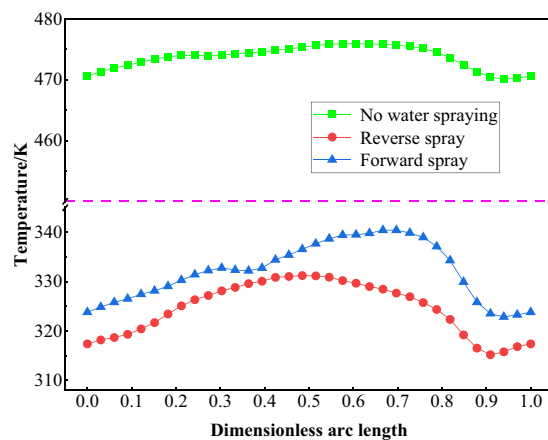**(A3) temperature under different conditions**

(A4a)20%THA

(A4b)10%THA

(A4c)5%THA

(A4d)3%THA

(A4) temperature under different conditions

Fig. 9 (continued)

The front and rear positions of the water spray nozzle with respect to different ways of spraying affect the temperature. Figure 9A1 and A2 correspond to the B1 and B2 curves before the water spray nozzle. The effect of reverse spraying is obvious, and the phenomenon is more obvious with the decline in load. The difference between the temperature distribution of the two types of water spray is 25 K-65 K. Figure 9A3 and A4 correspond to the B3 and B4 curves behind the water jet. The cooling effect of the two types of water jets has become weaker, not obvious in front of the water jet, but the cooling effect of the reverse spray is better than that of the downward spray. This phenomenon is due to the good atomization of water sprayed in the reverse spray method. The lower the load, the more back vortex flow and the reverse spray method of the surrounding fluid volume absorption capacity is stronger. Therefore, the droplets and steam contact area become larger, heat transfer capacity is enhanced, the proportion of evaporated droplets becomes larger, and the cooling effect is obvious.

3.4.3 The effect of the water spraying method on the cooling effect of the exhaust passage

The index of total temperature drop is chosen in this paper to quantitatively evaluate the effect of the water spraying method on the cooling effect of the exhaust passage. The total temperature drop coefficient can be defined as

$$\Delta T = T_{in} - T_{out} \tag{18}$$

where T_{in} is the average temperature of the inlet surface, K; T_{out} is the average temperature of the outlet surface, K.

Figure 10 shows the temperature drop of the exhaust passage. The temperature drop is negative when water is not sprayed, and the value of the temperature drop becomes smaller and smaller as the load decreases, indicating that as the load decreases, the steam flow in the exhaust passage decreases, the flow field in the passage becomes more complex, and the cooling capacity of the passage decreases, resulting in a significant increase in the outlet temperature. If the water spraying temperature drop is positive, the water spraying plays a cooling effect, and the evaporation of water droplets significantly reduces the exit temperature. The cooling effect of the reverse spray is better than the way down the spray, and the effect gradually becomes better with the decline in load. As can be seen from the Fig., the maximum difference between the temperature drop of the exhaust passage of the two spraying methods is 56.87 K. This is mainly due to the good atomization effect of the spraying water when reversing spraying, which is more conducive to the surrounding fluid volume absorption. Water droplets remain in the exhaust passage for a long time, contact steam for a long time, and are characterized by a long heat transfer time and good heat transfer effect.

4 Conclusions

The exhaust passage of the steam turbine is overtemperature during windage. In this paper, the Euler–Lagrange method was used to simulate multi-phase flows in sprays in

Fig. 10 ΔT under different conditions
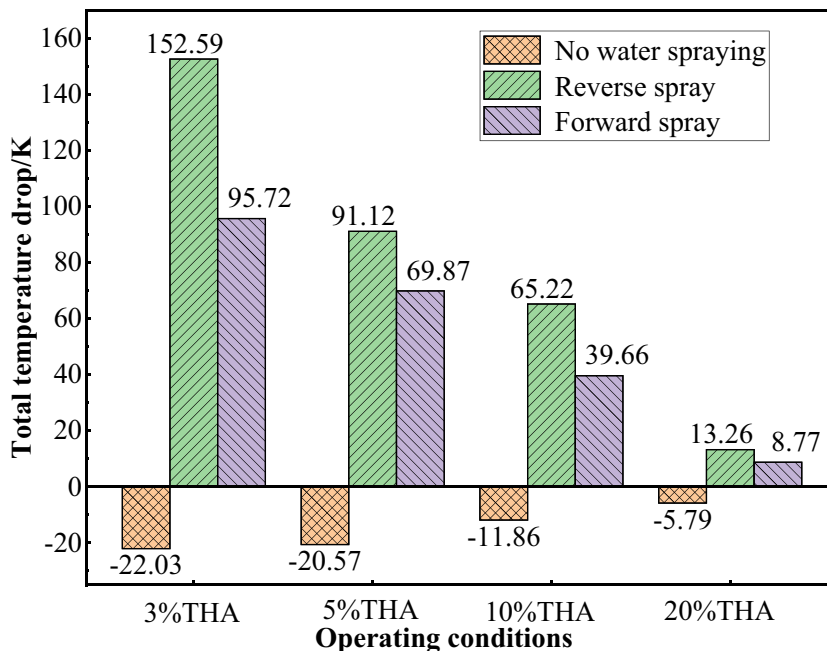
the exhaust passage of a 300 MW turbine. The flow field, aerorotor characteristics, and cooling effect of the exhaust passage were analyzed under blast conditions. The conclusions are as follows:

(1) This paper proposed a new type of water spraying arrangement for the exhaust passage, in which the water spraying ports are evenly arranged on the wall of the cone. Hence, the direction of water spraying is opposite to the direction of exhaust steam flow (reverse spraying), ensuring that the exhaust passage does not overheat when the steam exhaust of the turbine is lower than 20% THA blast condition. The evaporation amount of temperature reduction water under this arrangement (reverse spraying) is larger than the arrangement conFig.d by the manufacturer (downward spraying), and the maximum difference in evaporation amount is 0.42 kg/s.

(2) The change in aerorotor properties in the exhaust passage after water spraying results from the combined effect of evaporation of water-spraying droplets and droplet interference with the flow field. The pressure on the wall of the guide cone still increases along the axial length. However, the pressure on the wall of the guide cone near the water spraying port changes dramatically due to the impact of some unevaporated water droplets. The pressure on the wall of the guide cone still increases along the axial length. The total pressure drop is the largest when the backward spraying water droplets and exhaust vapor phase movement affect the static pressure recovery function of the exhaust passage. The maximum reduction of 8.17% in the static pressure recovery coefficient in the reverse spray mode increased the total pressure drop by 377.4 Pa.

(3) After the spray water temperature reduction, the vortex scale in the exhaust passage becomes larger, occupying the entire basin. In reverse spraying, back vortex flow increases, the surrounding fluid volume absorption ability is stronger, water droplets and steam contact for a longer time, heat transfer time is long, and a good temperature reduction effect is achieved. Furthermore, reverse spraying can reduce the temperature of the high-temperature zone of the leaf root, while smooth spraying can not. The maximum difference of 56.87 K between the temperature drop of the exhaust passage is achieved under the two spraying methods.

Declarations

References

1. Cao LH, Si HY, Dong EF et al (2018) Optimization of turbine discharge channel aerodynamic performance and analysis of condenser heat transfer characteristics. Chin J Electr Eng 38(12):3597–3604+19
2. Hu QL, Xu Q, Qian BY et al (2019) Influence of the diffuser tube shape modification design on the flow of steam turbine exhaust cylinder. Turbine Technol 61(04):250–253
3. Wang WY, Guo LD, An GY et al (2019) Flow characteristics analysis of steam turbine exhaust cylinder under small volume flow rate. Turbine Technol 61(01):43–46
4. Wang Z, Liu YM (2018) Analysis of the influence on the little volume flow condition for exhaust hood. Turbine Technol 60(05):332–334+339
5. Cao LH, Li LG, Hu HB et al (2020) Aerodynamic performance change of exhaust passage in steam turbine under low-load conditions. Int J Heat Mass Transf 157:1–10
6. Beevers A, Havakechian S, Megerle B (2015) On the prediction and theory of the temperature increase of low pressure last stage moving blades during low volume flow conditions, and limiting it through steam extraction methods. J Turbomach-Trans ASME 137(10):101002
7. Li MY, Wei CH, Liu WK et al (2020) Calculation and analysis of a low-pressure cylinder under small flow conditions and the corresponding retrofit measures. J Chin Soc Power Eng 40(03):206–212
8. Sureshkumar R, Kale SR, Dhar PL (2008) Heat and mass transfer processes between a water spray and ambient air–I. Experimental data. Appl Therm Eng 28(5–6):349–360
9. Sureshkumar R, Kale SR, Dhar PL (2008) Heat and mass transfer processes between a water spray and ambient air - II. Simulations. Appl Therm Eng: Des, Process, Equip, Econ 28(5–6):361–371
10. Sun YB, Alkhedhair AM, Guan ZQ et al (2018) Numerical and experimental study on the spray characteristics of full-cone pressure swirl atomizers. Energy 160:678–692
11. Montazeri H, Blocken B, Hensen JLM (2015) CFD analysis of the impact of physical parameters on evaporative cooling by a mist spray system. Appl Therm Eng 75:608–622
12. Xu MH, Cao LH, Luo HH et al (2020) Effect of water spray in exhaust passage of steam turbine on flow field of the last stage during windage. Int J Heat Mass Transf 161(1):120296
13. Xu MH, Cao LH, Si HY et al (2021) Effect of water spray in exhaust passage of steam turbine on aerorotor and strength performance of the last stage blade. Proc CSEE 41(07):2446-2454
14. Cao LH, Du H, Si HY (2021) Influence of water spray parameters on aerorotor characteristics and temperature drop characteristics of exhaust passage in steam turbine. Int J Heat Mass Transf 180:121829
15. ANSYS CFX help Theory Guide ANSYS18
16. Fan T, Xie YH, Zhang D et al (2007) Combined 3D numerical analysis of the low pressure exhaust hood coupling with the last two cascades in steam turbine. Proc CSEE 27(26):90-95
17. Fu WF, Liu K, Zhou LX (2017) Numerical simulation of the exhaust passage coupling with last stage in a 1000MW steam turbine. Proc CSEE 37(16):4722-4730+4897

18. Shao S, Deng QH, Shi HS et al (2013) Numerical investigation on flow characteristics in steam turbine low pressure cylinder and LPEH under different volume flow rate conditions. J Xi'an Jiaotong Univ 47(01):15–20

19. Vesilind PA (1980) The Rosin-Rammler particle size distribution. Resource Recov Conserv 5(3):275 (**Elsevier**)

20. Luo MC, Zheng Q, Sun LX (2012) The influence of inlet fogging for the stable range in a transonic compressor stage. J Eng Gas Turbines Power 134:1–11

21. Sun LX, Zheng Q, Luo MC et al (2011) On the behavior of water droplets when moving onto blade surface in a wet compression transonic compressor. J Eng Gas Turbines Power (134):1–10. https://doi.org/10.1115/1.4002822

22. You CF, Qi HY, Xu XC (2002) Research progress and application analysis of Basset force. J Appl Mech 19(2):31–3

23. Lin AQ, Zhou J, Fawzy H et al (2019) Evaluation of mass injection cooling on flow and heat transfer characteristics for high-temperature inlet air in a MIPCC engine. Int J Heat Mass Transf 882–894. https://doi.org/10.1016/j.ijheatmasstransfer.2019.02.025

24. Carey VP (1988) The properties of gases & liquids: 4th Edition. Exp Therm Fluid Sci 1(4):208–209

25. Cao H, Li Y, Si HY (2021) Research on temperature distribution characteristics in low pressure cylinder of large steam turbine under ultra-low load condition. Proc CSEE 41(03):1018-1026